Climate Dynamics (2020) 54:3583–3597
https://doi.org/10.1007/s00382-020-05182-w

Seasonal prediction of the northern and southern temperature modes of the East Asian winter monsoon: the importance of the Arctic sea ice

Peng Zhang[1,2,3] · Zhiwei Wu[1,3] · Jianping Li[4] · Ziniu Xiao[2]

Received: 20 July 2019 / Accepted: 20 February 2020 / Published online: 28 February 2020

Abstract
Previous research work found that two distinct surface air temperature (SAT) modes—the northern (N-) and the southern (S-) modes dominate the East Asian winter monsoon (EAWM) region. The inter-annual variations of these two modes were mainly attributed to preceding Siberian snow cover anomalies and El Niño–Southern Oscillation (ENSO). Observed evidence in this study shows that sea ice anomalies on Barents–Kara (BK) and Laptev Seas and those on Chukchi–Beaufort (CB) Sea in autumn have co-mingled effects on the two abnormal EAWM modes. If negative sea ice anomalies appear in the BK and northern CB Sea in September–October (SO), the following winter SAT anomaly over East Asia is featured by an obvious cooling north of 40° N, which highly resembles the SAT N-mode of EAWM. If negative sea ice anomalies occur in BK–Laptev Sea but positive anomalies in the southern CB Sea, the East Asia winter SAT anomaly exhibits a salient cold condition over the south of 40° N and corresponds to the EAWM S-mode. The above results indicate that autumn Arctic sea ice can provide another predictability source for the EAWM, besides Siberian snow cover and ENSO. To further verify its contribution to seasonal prediction of the EAWM, a series of physical–empirical models are established using the combinations of SO Arctic sea ice, autumn Siberian snow cover and ENSO. Hindcast experiment output shows when adding autumn Arctic sea ice into the predictors, the cross-validated prediction skill is significantly improved. The possible physical mechanisms on how preceding Arctic sea ice anomalies impact on the N- and S- modes are also discussed.

1 Introduction

As a vigorous atmospheric system during boreal winter, the East Asian (EA) winter monsoon (EAWM) exerts a great impact on the EA winter climate and has garnered widely attentions (Tao 1957; Wang et al. 2000; Chen et al. 2014; Wang and Chen 2014 and many others). The cold surge activity and surface temperature (SAT) fluctuations induced by the variation of EAWM always exert obvious influence on people's production and life (Lau and Li 1984; Ding 1994; Chen et al. 2000). The seasonal forecast of EAWM is thus increasingly being recognized as essential for social and economic development. However, due to the chaotic nature of atmosphere and uncertainties in the model parameterizations of sub-grid scale processes, dynamical seasonal predictions for summer or winter SAT and precipitation in the EA regions still exhibit poor skills (Wang et al. 2009; Lee et al. 2013). Recent years, several studies attempted to predict the EAWM through establishing a physically-based empirical model, and obtained a considerable prediction skills (Wu et al. 2011; Lee et al. 2013; Zuo et al. 2016; Yu et al. 2018), indicating the statistical prediction an effective strategy for improving the ability of EAWM seasonal prediction.

A simple and representative index is of great importance for the statistical seasonal prediction of EAWM (Wang and Chen 2014). However, a single index is hard to seize the EAWM variability over the entire EAWM domain (Wang and Chen 2010; Liu et al. 2012). Because of the sizeable meridional extent, EAWM may present distinct variation

✉ Zhiwei Wu
zhiweiwu@fudan.edu.cn

1 Department of Atmospheric and Oceanic Sciences, Institute of Atmospheric Sciences, Fudan University, 2005 Songhu Rd, Yangpu, Shanghai 200438, China

2 State Key Laboratory of Numerical Modeling for Atmospheric Sciences and Geophysical Fluid Dynamics, Institute of Atmospheric Physics, Chinese Academy of Sciences, Beijing 100029, China

3 Shanghai Key Laboratory of Meteorology and Health, Shanghai 200030, China

4 Laboratory for Regional Oceanography and Numerical Modeling, Qingdao National Laboratory for Marine Science and Technology, Qingdao 266237, China

characteristics between the tropical and mid- to high-latitude EA region. For example, Wang et al. (2010) revealed that the abnormal SAT in the EAWM region is controlled by the northern (N-) and the southern (S-) modes, which have obvious different circulation structures and sources of variability, leading to accordant and diverse winter climate anomalies between the mid- to high-latitude and tropical EA regions in different years. Therefore, distinguishing the N- and S-modes of the EAWM for a better prediction of the climate anomalies over the entire EAWM domain calls for more considerations and discussions.

Previous studies found the variations of Eurasian snow cover (Gong et al. 2003; Jhun and Lee 2004; Cohen et al. 2014; Luo and Wang 2018), sea ice in Arctic (Honda et al. 2009; Li and Wang 2014; Wu et al. 2015; Zuo et al. 2016), El Niño–Southern Oscillation (ENSO) (Zhang et al. 1996; Wang et al. 2000, 2008; Zhang et al. 2017, 2019a) and the Southern Annular Mode (Wu et al. 2009) contribute to the variability of EAWM. For the two SAT leading modes of EAWM, Wang et al. (2010) suggested that the cold N-mode is preceded by excessive autumn southern Siberian snow cover (SSSC), whereas the cold S-mode is attributed to the development of cold ENSO events and less northeastern Siberian snow covers (NESSC). Nevertheless, several studies have found an unstable connection between ENSO and EAWM (He and Wang 2013; Jia et al. 2016) and only a part of temperature variability over EA can be explained by the anomalous Eurasian snow cover (Clark and Serreze 2000, Luo and Wang 2018). Furthermore, if checking the time series of winter N-mode, S-mode, the preceding autumn SSSC, Niño3.4, and NESSC indices as well as the temporal correlation coefficients (TCC) among them in Fig. 1c, d, we also found that neither the autumn Siberian snow cover nor ENSO can explain the variance of SAT N-mode or S-mode of EAWM by more than 20%. Therefore, other precursors and the associated mechanisms are required so as to further improve the prediction of the two SAT leading modes of EAWM.

As an indispensable constituent of the global climate system, the variation of Arctic sea ice and its related Arctic warming could induce the local and remote large scale circulation and climate anomalies in the Northern Hemisphere via modulating the storm tracks, the jet stream, the phase of North Atlantic Oscillation (NAO)/Arctic Oscillation (AO), and the upward and horizontal propagating planetary waves (Budikova 2009; Overland and Wang 2010; Petoukhov and Semenov 2010; Francis and Vavrus 2012; Hopsch et al. 2012; Inoue et al. 2012). Therefore, more and more studies emphasized the influence of Arctic sea ice (Tang et al. 2013; Mori et al. 2014; Vihma 2014; Wu et al. 2016). Especially, the impact of Arctic sea ice and its associated atmospheric anomalies on EA climate have long been concerned (Wu et al. 1999; Kug et al. 2015). Wu et al. (1999) found an intimate connection between less autumn Arctic sea ice and the strong EAWM. Honda et al. (2009) revealed that a decline in Arctic sea ice along the Eurasian coast in September could intensify the Siberian High in the following December and lead to the cold temperature anomalies appear over the EA region. Moreover, the anomalous Arctic sea ice could also induce a negative phase of NAO that results in a widespread cooling over mid-latitude Eurasia during the late winter. Francis et al. (2009) pointed out that less early autumn sea ice in the Arctic tends to slack the poleward atmospheric thickness gradient, weakening the polar jet stream. Such a declined polar jet stream favors the polar region cold air coming down to the mid-latitude EA region (Wu et al. 2015; Sun et al. 2016). The Arctic sea ice, therefore, is believed an early indicator of variations occurring in the North Hemisphere climate (Solomon et al. 2007), which may provide potential predictability of about one season (Chevallier and Salas-Melia 2012).

However, the previous studies did not discuss whether and how the abnormal autumn Arctic sea ice exerts its influence on the SAT N-mode and S-mode of EAWM, respectively. Meanwhile, their attentions were mainly paid to the impact of Eurasian Arctic, for instance, the Barents–Kara Seas, the Laptev Seas. As a matter of fact, the Chukchi–Beaufort sea ice experienced the fastest rate of decrease and strongest interannual variance than anywhere in the Arctic (Zhang and Walsh 2006; Zhang et al. 2008, 2018; Stroeve et al. 2011; Comiso 2012). Therefore, this article attempts to explore the abnormal autumn sea ice in both Eurasian Arctic and Chukchi–Beaufort Seas, which exert a great impact on the winter SAT in the northern and southern EA. On this basis, clarifying to what extent they contribute to the seasonal prediction of the SAT N- and S-modes of EAWM. The manuscript is framed as follows. Section 2 introduces the data and methods applied in this study. The distinct principle modes of EA winter SAT variability, as well as how the autumn Arctic sea ice impact on these two modes, are discussed in Sects. 3 and 4. Section 5 introduces the empirical models that are established based on sea ice indices. Section 6 includes a conclusion and discussion.

2 Data and methodology

The datasets used in this study including (1) the ERA-interim reanalysis data at $1.5° \times 1.5°$ horizontal resolution, available from the European Centre for Medium-Range Weather Forecasts (ECMWF; Dee et al. 2011); (2) the sea ice concentration (SIC) dataset gridded at $1.0° \times 1.0°$ resolution ranging from September 1979 to February 2018 are provided by Met Office Hadley Centre (Rayner et al. 2003); and (3) the Global Snow Lab (Rutgers University)

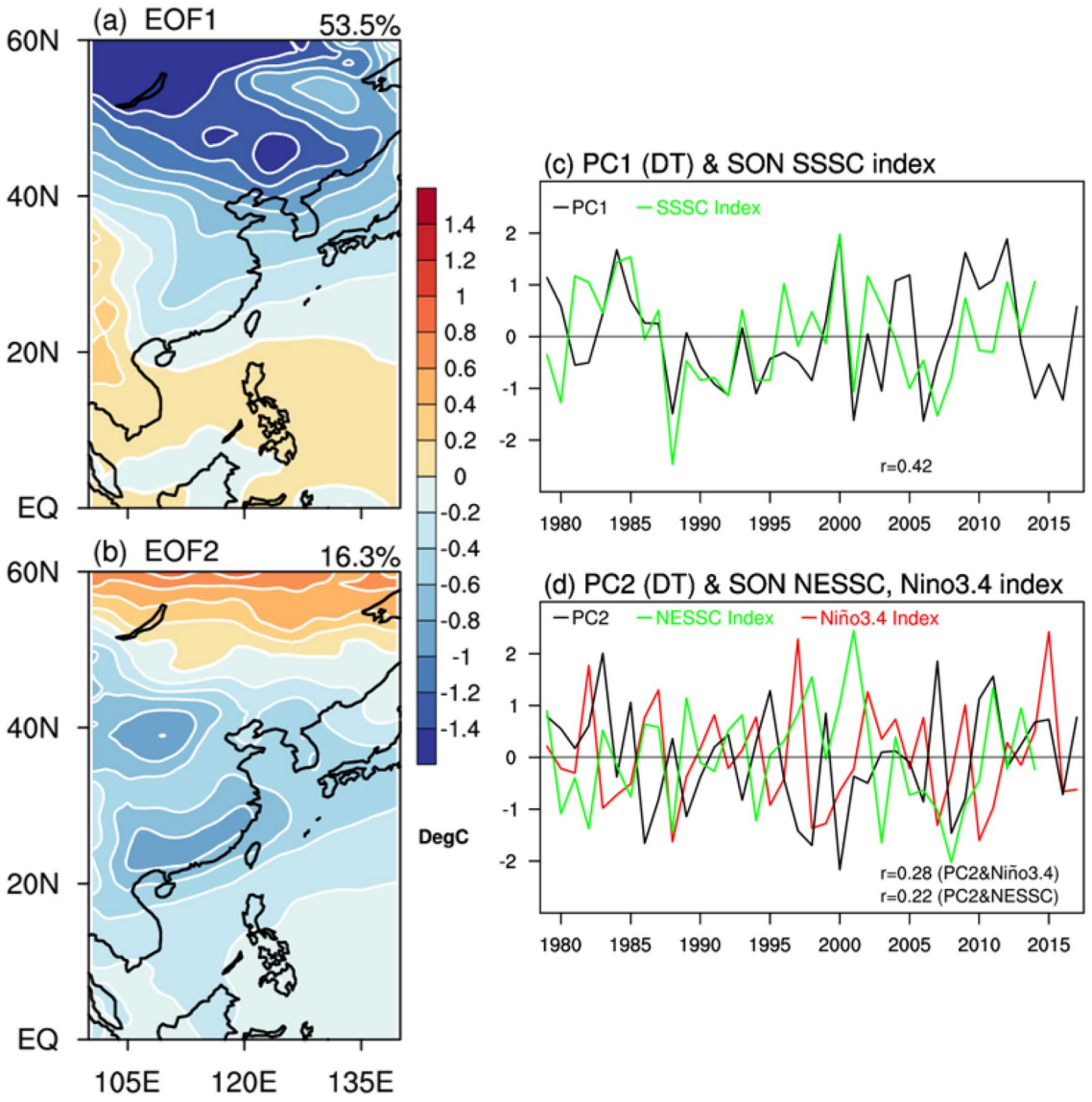

Fig. 1 Spatial patterns (°C) of the first and the second **a**, **b** EOF mode of the winter mean 2-m air temperature in the entire EAWM domain. **c** PC1 (black) and Southern Siberian snow (green) index, **d** PC2 (black), Nino3.4 (red) and Northeastern Siberian snow cover (green) indices

monthly North Hemisphere snow cover datasets (http://climate.rutgers.edu/snowcover; Robinson et al. 1993; Robinson and Frei 2000; Estilow et al. 2015) ranging from September 1979 to February 2016; (4) Niño3.4 index (defined within the area of 5° N–5° S, 120° E–170° W) obtain from the Climate Prediction Center (CPC). Following the definitions given by Wang et al. (2010), the fall southern Siberian snow cover and the northeastern Siberian snow cover indices refer to the averaged snow cover anomalies within the regions of 45°–60° N, 70°–140° E and 60°–70° N, 130°–180° E, respectively. The data and indices applied in this study are de-trended to avoid the disturbance of the linear trend.

3 Distinct principal modes of EA winter SAT variability

To understand the connection of Arctic sea ice and EA winter surface temperature (SAT) anomalies, first, we carried out EOF analysis of the SAT anomalies over the EAWM region (0°–60° N, 100°–140° N) and checked the SAT leading modes. The spatial structures and the corresponding PCs of the two principal modes are displayed in Fig. 1. Both PC1 and PC2 represent a salient interannual variability and explain 53% and 16% of the total variance. The North's test (North et al. 1982) proved that they are significantly distinguished from each other. For the EOF1, a negative loading center locates over the north of 40° N with the intensity of

the negative anomalies decreasing southward, switching to the positive anomalies around 20° N. Such a pattern reflects the invasion of the cold air mass into the northern EA. For the EOF2, the negative loading centers located over the south of 40° N with the positive anomalies appear to the north of 50° N, signifying the cold air intrudes into southern EA. The EOF1 and EOF2 are thus named SAT Northern (N-) mode and the Southern (S-) mode. Both the spatial patterns and the time series of SAT N-mode and S-mode of EAWM share similar features of that given by Wang et al. (2010).

It is of interest to investigate the discrepancy of the dynamic structures associated with the N-mode and the S-mode. Regression shows that the simultaneous atmospheric circulation of N-mode highly resembles the negative phase of AO with a stronger than normal Siberian–Mongolian High as well as a deepening EA trough over the Lake Baikal (Fig. 2a, b). The S-mode is accompanied by a reinforced and southward shifted EA trough and an enhanced continental surface high pressure over Mongolia with its ridge extending southward down to southern China (Fig. 2c, d). As the spatial patterns and the associated atmospheric anomalies represent large differences between the winter SAT N-mode and S-mode, what is the relationship between the preceding autumn Arctic sea ice and these two principal modes?

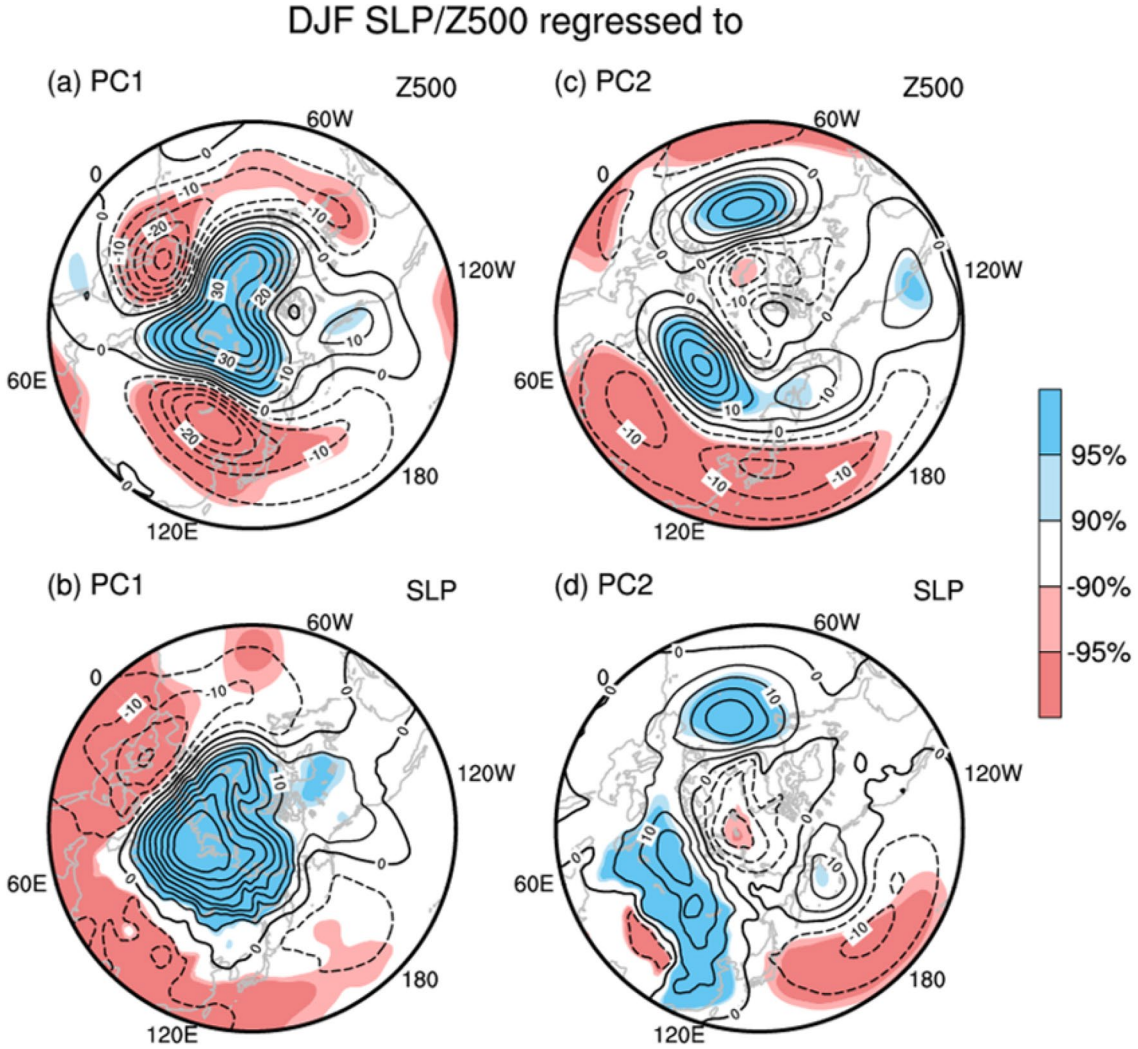

Fig. 2 SLP (Pa), Z500 (m) anomalies regressed with reference to **a**, **b** PC1 and **c**, **d** PC2. The dark (light) shaded regions represent positive (negative) values exceeding 95% (90%) confidence level (Student's t test)

4 Impact of autumn Arctic sea ice

4.1 Distinct abnormal autumn Arctic sea ice patterns associated with N- and S-mode

To answer the abovementioned question, Fig. 3 examines the autumn sea ice anomalies associated with these two principal modes. It shows that the cold SAT N-mode is preceded by the significant abnormal negative sea ice in the Barents–Kara (BK) Sea and the North Chukchi–Beaufort (N-CB) Sea in September–October (SO) (Fig. 3a). If the sea ice concentration (SIC) averaged within the framed regions in the BK Sea (78.5°–82.5° N, 35°–100° E) and N-CB Sea (72.5°–77.5° N, 175°–205° E) is defined as BK index (BKI) and N-CB index (N-CBI), the correlation between BKI and N-CBI is − 0.08, indicating they are independent of each other. For the cold S-mode, the loss of autumn sea ice is also detected in the BK Sea and the anomalies stretch to the Laptev Sea, but the salient positive sea ice anomalies appear in the South CB (S-CB) Sea instead of the negative anomalies over the N-CB region for the N-mode (Fig. 3b). Therefore, we defined the averaged SIC in the BK (78.5°–82.5 °N, 35°–100 °E, BKI) and Laptev (77.5°–83.5° N, 120°–150° E) Sea as the Beaufort–Kara–Laptev index (BKLI). Defining averaged S-CB (71.5°–73.5° N, 185°–210° E) sea ice as the S-CB index, which is independent of BKLI (TCC of them is 0.05).

The previous study found the different regional Arctic sea ice may exercise a distinct influence on the distant atmospheric circulation (Koenigk et al. 2016). Figure 4 compares the winter sea level pressure (SLP), 500-hPa geopotential height (Z500) and SAT anomalies associated with the abnormal SO sea ice in the BK, BKL, South and North CB Seas. It is noticed that the circulation anomalies induced by reduced BK and BKL sea ice share a striking similar spatial pattern. The PCCs of the Z500, SLP and SAT anomalies induced by the abnormal BK (Fig. 4a–c) and BKL (Fig. 4d–f) sea ice are 0.93, 0.92 and 0.95, respectively. These patterns are reminiscent of the remote responses to the anomalous sea ice along the Eurasian Arctic as discussed by Wu et al. (2015) and Zuo et al. (2016), who found the decreased abnormal autumn Eurasian Arctic SIC tend to strength the winter Siberian High (SH) and EA trough, favoring the cold air masses intrude southward from high-latitude and thus cold condition overs entire China.

Next, we investigate the impacts of the anomalous sea ice in the CB Sea. When the SO sea ice anomalies decrease in

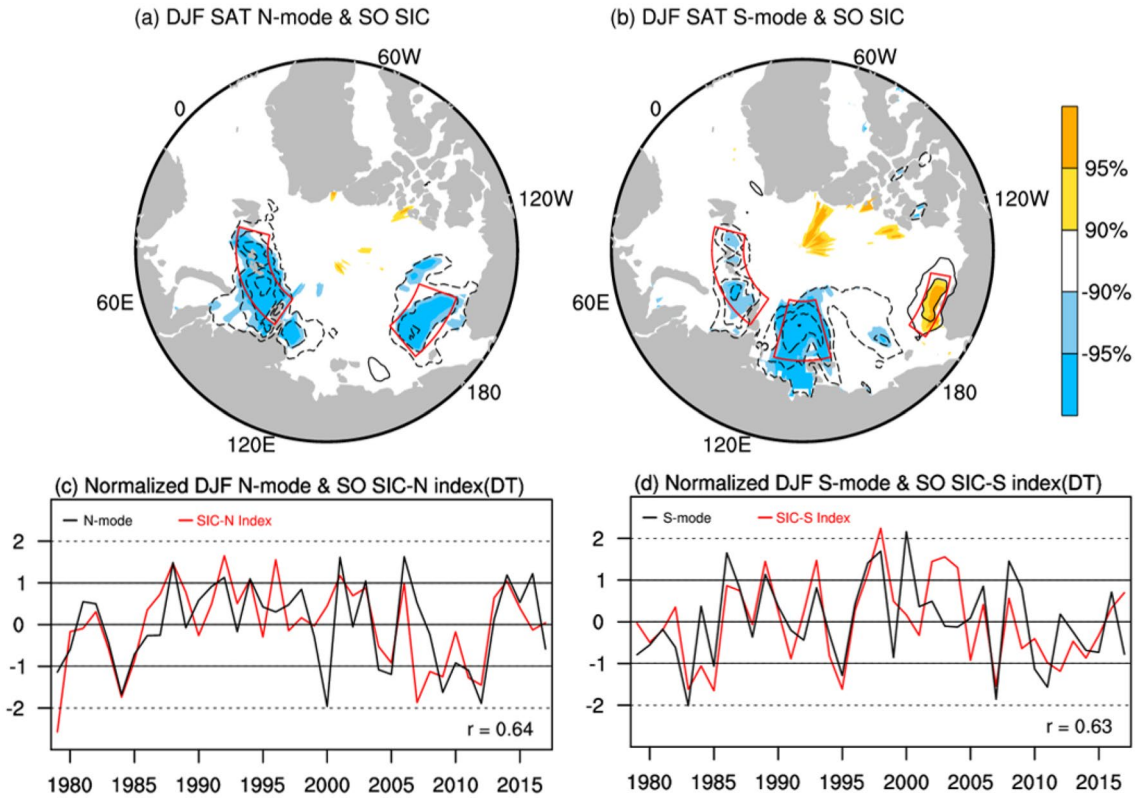

Fig. 3 SO(0) SIC anomalies regressed with reference to **a** PC1 and **b** PC2. The shading regions represent values exceeding 95% (90%) confidence level (Student's t test). The time series for **a** PC1 (black) and N-mode-related SIC (SIC-N; red) indices, **b** PC2 (black) and S-mode-related SIC (SIC-S; red) indices

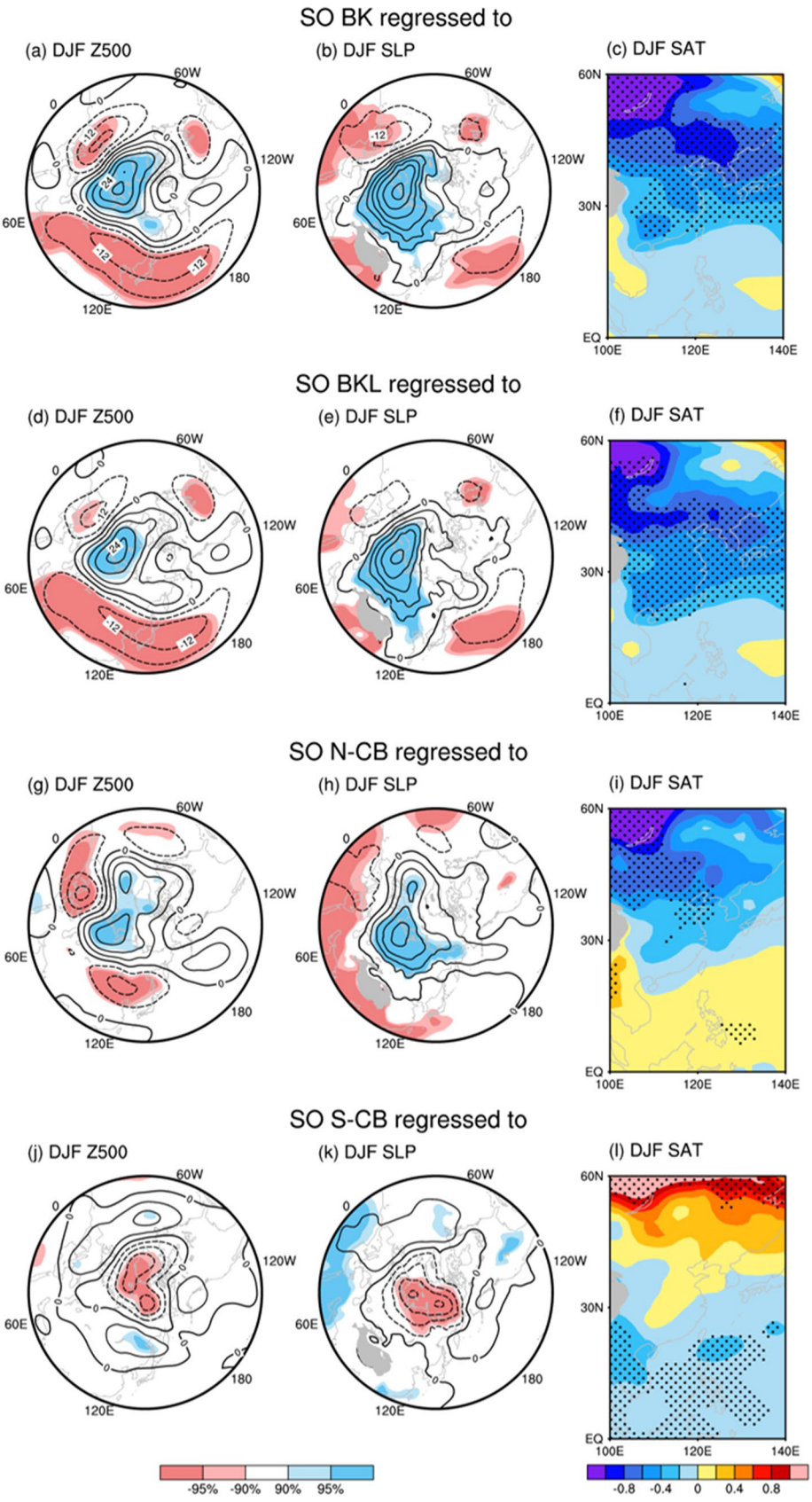

Fig. 4 DJF(1) SLP (hPa), Z500 (m) and SAT (°C) anomalies regressed with reference to SO(0) BKI (**a**–**c**), BKLI (**d**–**f**), N-CBI (**g**–**i**), and S-CBI (**j**–**l**). The dark (light) shaded regions in **a**, **b**, **d**, **e**, **g**, **h**, **j**, **k** represent positive (negative) values exceeding 95% (90%) confidence level. The dots region in **c**, **f**, **i**, **l** represent values exceeding 95% confidence level (Student's t test)

the N-CB Sea, significant positive Z500 and SLP anomalies appear over the Ural region in the following winter, indicating the intensive Ural Blocking high (Fig. 4g), which can reinforce the cold advection downstream that enhances the SH (Fig. 4h) (Lu and Chang 2009). Meanwhile, an obvious negative Z500 anomaly center is seen over the Lake Baikal (Fig. 4g). The corresponding SAT anomalies in the wintertime exhibit a dipole mode with the cold polarity controlling the northern EA and the warm polarity over the southern EA (Fig. 4i). For the positive S-CB sea ice anomalies (Fig. 4j–l), the corresponding spatial distributions of Z500, SLP, and SAT are approximately contrary to that of negative N-CB sea ice anomalies (Fig. 4g–i). In Z500, an anomalous high pressure, replacing the anomalous low in Fig. 4g, appears over the Lake Baikal (Fig. 4j). Over the polar region, the anomalous low in the middle to lower troposphere indicates a reinforced polar vortex (Fig. 4j, k). The resultant SAT anomalies (Fig. 4l) show a meridional reversed dipole mode compared with that of the negative N-CB sea ice anomalies (Fig. 4i).

As the reduced BK and BKL sea ice share a striking similar circulation anomalies pattern, the autumn sea ice conditions over the CB Sea may modulate the influences of abnormal Eurasian Arctic sea ice on the SAT leading modes of EAWM. In the next part, we will discuss such modulating effects of CB sea ice using combined sea ice indices.

4.2 The modulation effects of abnormal autumn sea ice in the CB Sea

Considering the simultaneous but independent variations of the sea ice in the Eurasian Arctic and the Chukchi–Beaufort Sea. We used multiple regression method to build the combined sea ice indices. First, we conducted normalization to the BKI, BKLI, N-CBI and the S-CBI. Second, we performed multiple regression analysis based on the normalized indices:

$$Y = a_1 \times X_1 + a_2 \times X_2 + \cdots + a_n \times X_n$$

where Y is a normalized EAWM N-mode or S-mode index; X_1, X_2,…, X_n are the different sea ice indices; a_1, a_2,…, an are the regression coefficients. Depended on the regression coefficients, we established two sea ice concentration indices which related to the EAWM N-mode and S-mode, respectively:

$$\text{SIC-N} = 0.49 \times \text{BKI} + 0.40 \times \text{N-CBI}$$

$$\text{SIC-S} = 0.51 \times \text{BKLI} - 0.32 \times \text{S-CBI}$$

The newly established N-mode related sea ice (SIC-N) index shows a high correlation with the SAT N-mode (Fig. 3c). The TCC between them is 0.64, which exceeds the 99% confidence level based on a Student's t test. For the S-mode related sea ice (SIC-S) index (Fig. 3d), the TCC between it and SAT S-mode is 0.63, which also exceeds the 99% confidence level based on a Student's t test. Figure 5 compares the spatial pattern of winter Z500, SLP, and SAT anomalies corresponding to the SIC-N and SIC-S indices. For the SIC-N anomalies, the autumn negative sea ice anomalies in the BK Sea induce a deepening EA trough extending from Mongolia to the ocean east of Japan in winter and the loss of N-CB sea ice corresponding to the negative Z500 anomalies over the Lake Baikal. Their combined effect makes the prominent negative Z500 anomalies stronger over the Lake Baikal (Fig. 5a). It is known that the climatological EA trough tilts southwestward from the Kamchatka peninsula to Japan, the abnormal low close to Lake Baikal indicates a northwestward shifted EA trough. Meanwhile, a much more powerful Ural blocking and Siberian High are detected in boreal winter in response to the commingle forcing of autumn BK and N-CB sea ice anomalies (Fig. 5a, b). Such circumstance favors the cold spell from the polar area converges to the northern EA, inducing a colder than normal winter there, but a relatively warmer condition prevailing in the southern EA (Fig. 5c). The pattern correlation coefficient (PCC) between the SAT anomalies corresponding to PC1 (Fig. 1a) and SIC-N index (Fig. 5c) is 0.97, implying the anomalous SAT pattern in Fig. 5c can explain around 94% of the N-mode signal.

For the SIC-S index, the related wintertime atmospheric anomalies differ from that of SIC-N. Although the loss of autumn BKL sea ice can enhance the Siberian High and EA trough in the following winter, the increased S-CB sea ice generates an abnormal low over the polar region and an anomalous high over the Lake Baikal. Thus, the spatial pattern in Fig. 5d–f reflect a superimposing impact of the SO BKL and S-CB sea ice anomalies. In the mid-troposphere, a salient anomalous centered over the Ural regions with the significant low-pressure anomalies sited over southern Japan, corresponding to an enhanced Ural blocking high and a southward shift of EA major trough (Fig. 5d). The significant positive SLP anomalies (Fig. 5e) appear over the Siberia regions with a salient SLP ridge elongates from central Siberia southeastward to southern China. Meanwhile, a notable abnormal low appears over the subtropical North Pacific. Such large zonal gradient between the abnormal surface subtropical North Pacific low and the EA continental high favor the northerly anomalies penetrating from Siberian region to the South China Sea, leading to a cold condition dominates the southern EA (Fig. 5f), resembling the SAT S-mode (Fig. 1b). The PCC of them is 0.87, meaning the anomalous SAT pattern in Fig. 5f can explain about 77% of the S-mode signal.

Therefore, the above results imply that the SAT N-mode and S-mode of EAWM attribute their existence to a

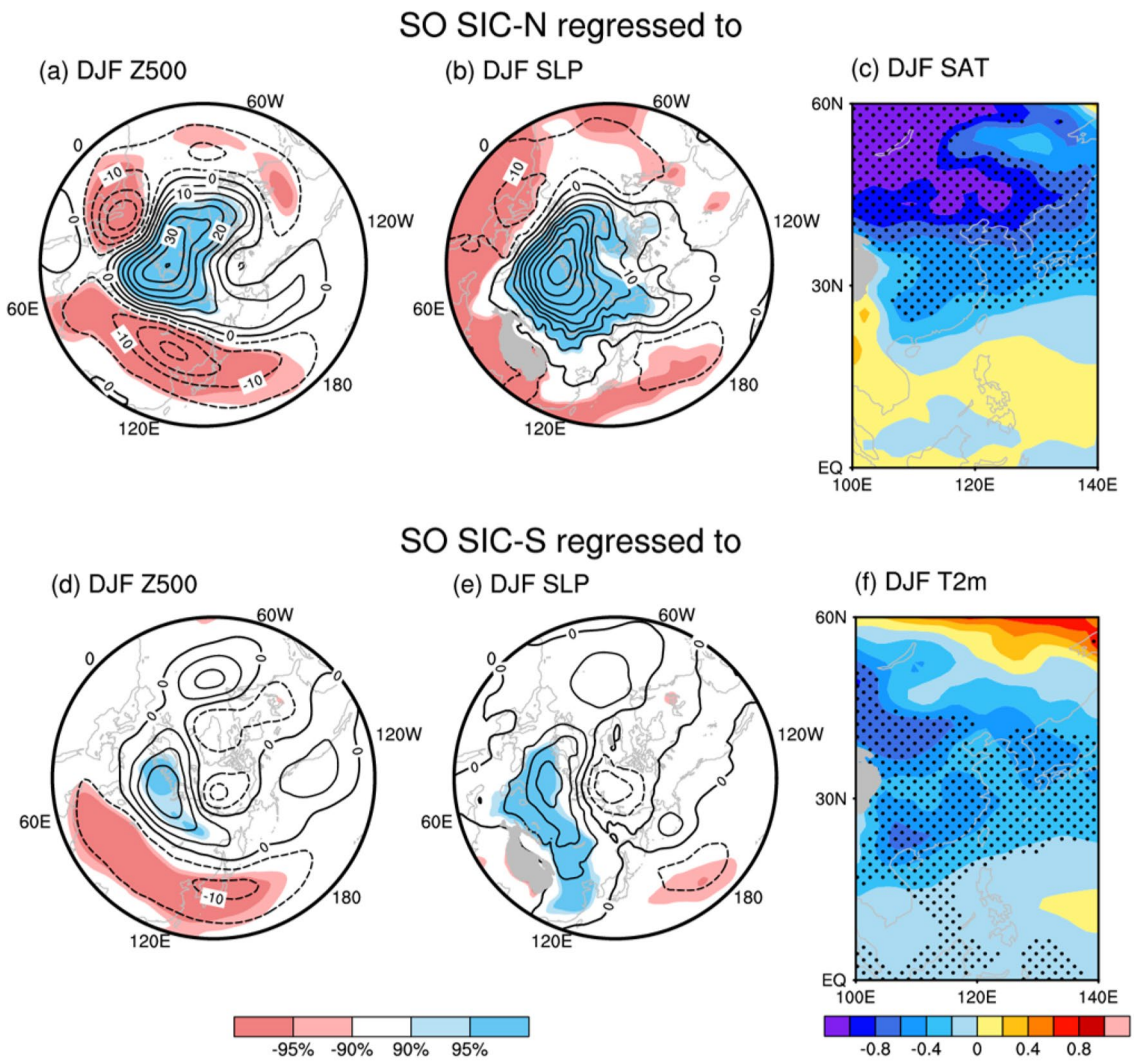

Fig. 5 Same as Fig. 4 except for SO (0) SIC-N (**a**–**c**) and SIC-S (**d**–**f**) indices

superposition of the independent effects of anomalous sea ice in the Eurasia Arctic and Chukchi–Beaufort Sea.

4.3 The influencing processes of SIC-N and SIC-S anomalies on N- and S-mode

The aforementioned analysis has presented the connection of autumn SIC-N and SIC-S anomalies and SAT N- and S-mode of EAWM. Still unclear is what process drives such a connection? Many studies attributed the recent continental cold winters to Arctic warming (Screen et al. 2013; Screen 2014; Cohen et al. 2014). For example, Kug et al. (2015) revealed that the anomalous warmth in the Barents–Kara Sea and East Siberian–Chukchi Sea regions might result in severe winter in East Asian and North America, respectively. Figure 6 shows the regression maps between autumn SIC-N and SIC-S indices against DJF SAT anomalies and between N- and S-mode against SO SAT anomalies. For SIC-N anomalies, with the sea ice decreases in the BK and N-CB Seas in autumn, an anomalous positive SAT is seen over the eastern Arctic in the following winter (Fig. 6a). It is interesting to notice that the salient positive SAT anomalies associated with SAT N-mode also appear in the eastern Arctic (Fig. 6c). An N-mode-related temperature index (NTI) is constructed as the standardized area-averaged SAT anomalies within the boxed region (76°–86° N, 0–70° E) to measure the variability of SAT over the east of Arctic. To check whether the SAT anomaly in this region has a persistent connection with the SIC-N and N-mode, the lead-lag TCCs between temperature index (NTI) and N-mode (red solid curve), SIC-N (blue solid curve) and between SO temperature index and temperature index (black solid curve) from SO to DJF are displayed in Fig. 7. The TCCs between them are significant at 95% of confidence in autumn and persist

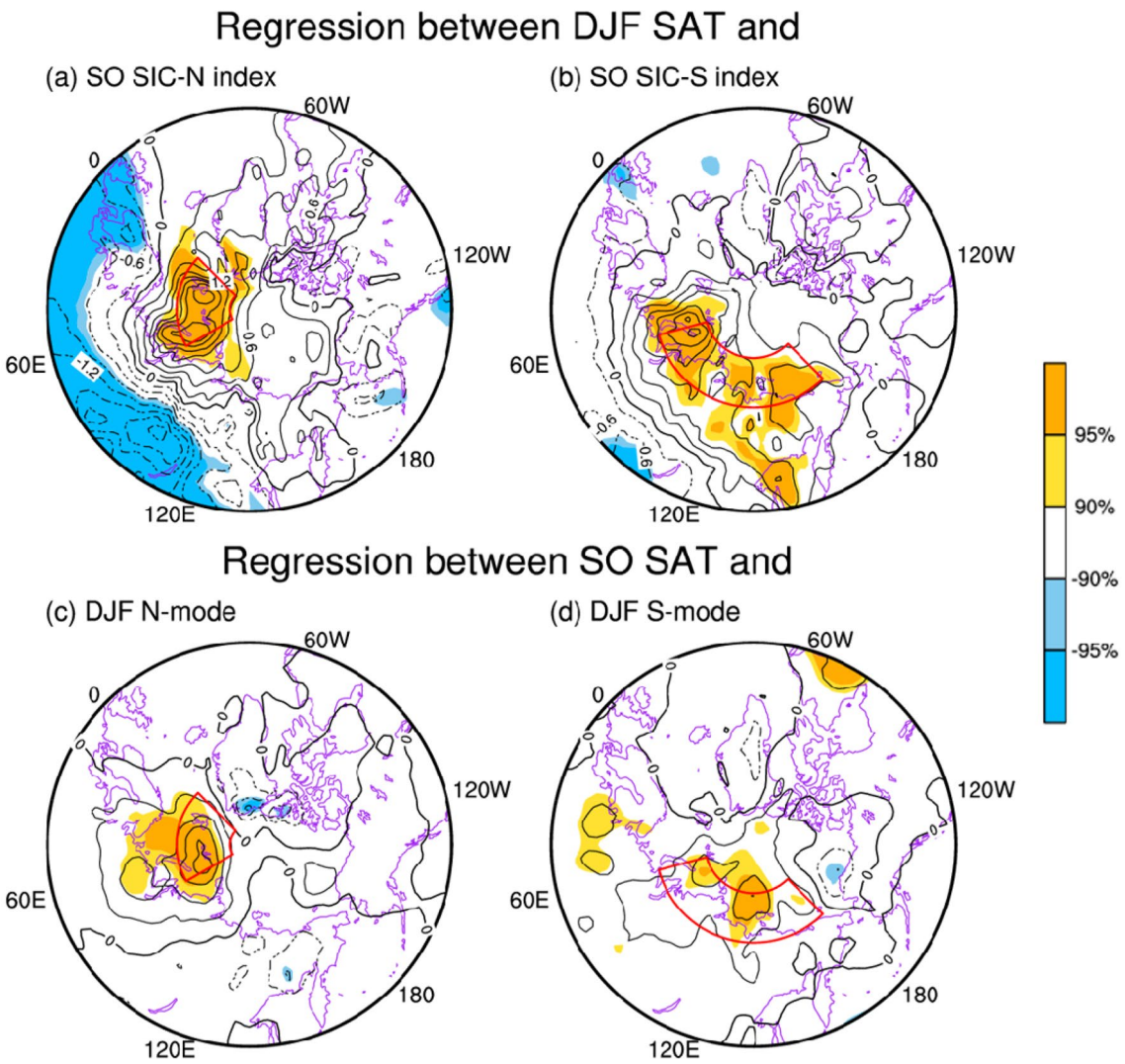

Fig. 6 DJF(1) SAT (°C) anomalies regressed with reference to the SO(0) SIC-N (**a**), SIC-S (**b**) indices, and SO(0) SAT (°C) anomalies regressed with reference to the DJF(1) S-mode (**c**), N-mode (**d**) indices. The dark (light) shaded regions represent positive (negative) values exceeding 95% (90%) confidence level (Student's t test)

to the following winter, implying the persistent warmth in the eastern Arctic connects the SIC-N anomalies in autumn and the SAT N-mode.

For the SIC-S, whereas, there is a salient reduction of sea ice over the BKL Sea but an increase in the S-CB Sea during autumn, which is followed by anomalous warm conditions in the Eurasian Arctic and Northern Continent (Fig. 6b). Figure 6d present the regression pattern between PC2 (S-mode) and preceding autumn SAT anomalies. Generally, the salient anomalous positive SAT is still sited over the Eurasian Arctic and Northern continent, which highly resemble that of Fig. 6b. An S-mode-related temperature index (STI) is calculated as the temperature anomalies averaged within the red box in Fig. 6b, d (70°–82° N, 60°–170° E). The dash curves in Fig. 7 shows the corresponding lead-lag TCCs. The significant TCCs persist from SO to the following winter, indicating the SO SIC-S anomalies and S-mode can be linked by the persistent warmth in the Eurasian Arctic and Northern continent.

The greater than normal temperature caused by reduced Arctic sea ice contribute to an expansions in the local 1000–500-hPa thickness field, which may result in a weakened meridional gradient in 1000–500-hPa thickness between Eurasia and polar region and further reduce the zonal wind over mid- to high-troposphere (Francis et al. 2009; Overland and Wang 2010). Figures 8 and 9 compared the SAT, 1000–500 hPa thickness, and U500 anomalies from SO to DJF that associated with SIC-N and SIC-S indices, respectively. During autumn, in conjunction with the SIC-N and SIC-S anomalies, salient positive SAT occur over the eastern Arctic

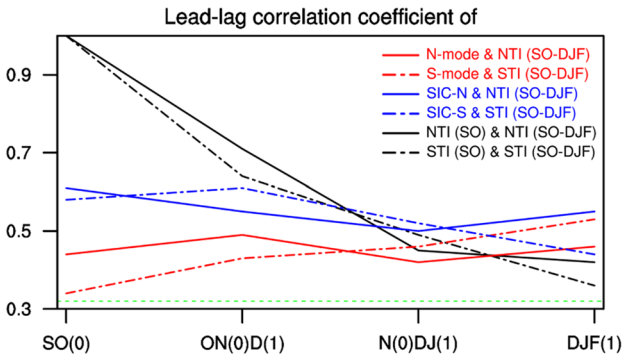

Fig. 7 The lead-lag correlation coefficient between DJF(1) N-mode (red solid line), SO(0) SIC-N (blue solid line), SO(0) NTI (black solid line) and NTI from SO(0) to DJF(1), between DJF(1) S-mode (red dash line), SO(0) SIC-S (blue dash line), SO(0) STI (black dash line) and STI from SO(0) to DJF(1). The green dash line represents the 95% confidence level based on Student's t test

(Fig. 8a) and over the Eurasian Arctic and Northern Continent (Fig. 9a). The appearance of two types of Arctic warming that related to the SIC-N and SIC-S indices is about one season ahead of the two EA SAT modes in winter (Figs. 8d, 9d). Examining the simultaneous 1000–500-hPa thickness anomalies associated with the SIC-N index, it shows that the thickness increases over the eastern Arctic (Fig. 8e), inducing a negative U500 anomaly prevailing along the 70° N (Fig. 8i). Comparing with the SIC-N anomalies, the SIC-S-related 1000–500-hPa thickness anomalies move southward to the Eurasian Arctic and Northern Continent (Fig. 9e), the resultant negative U500 anomalies that also southward shifted to the 50° N (Fig. 9i). And then, with the two types of SAT anomaly over the Arctic that persist from SO to DJF (Figs. 8, 9, upper panel), the resultant positive 1000–500 hPa thickness anomalies over the Arctic also show strong seasonal persistence (Figs. 8, 9, middle panel), decreasing the U500 over the mid-high latitude Eurasian from autumn to winter (Figs. 8, 9). It is known that the amplitude and speed of large scale Rossby waves can be affected by zonal wind. The eastward

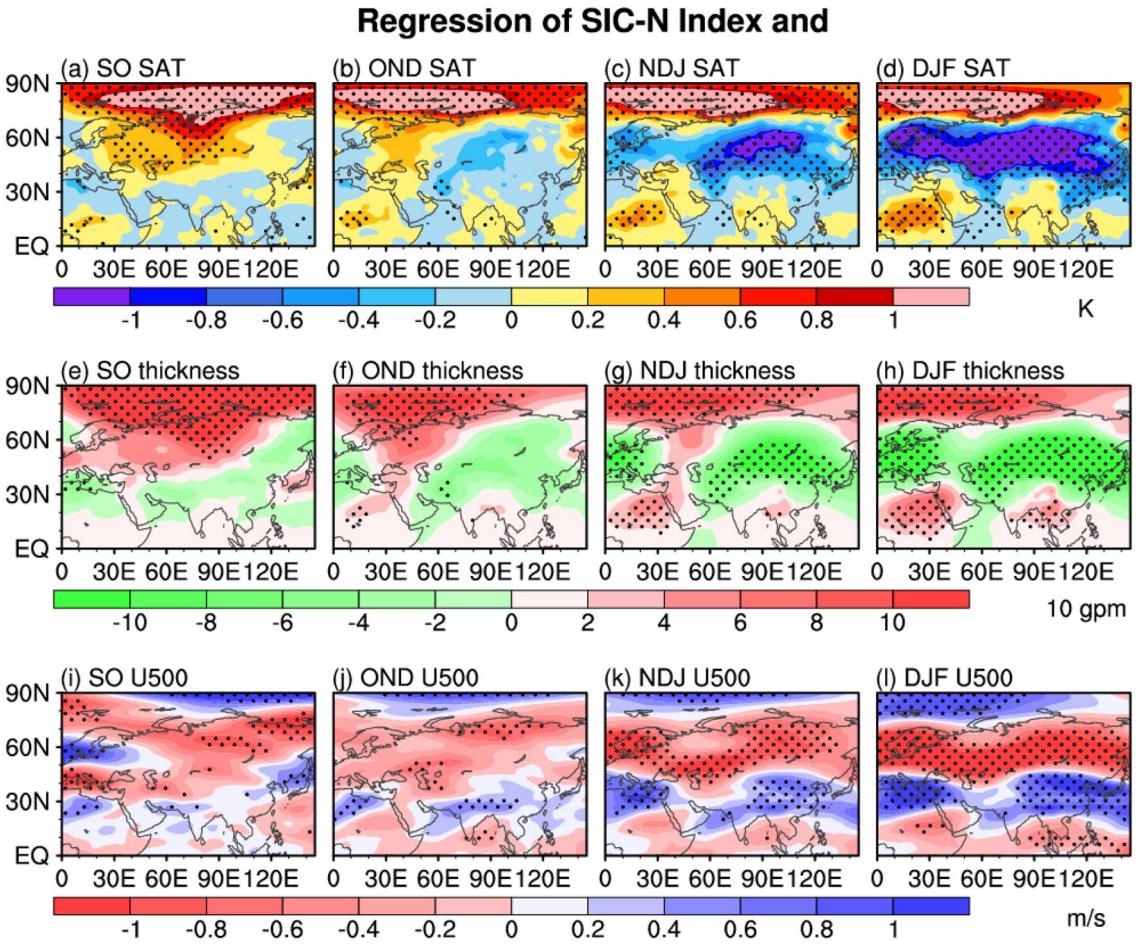

Fig. 8 Regression of SO SIC-N index and SAT anomalies for **a** SO, **b** OND, **c** NDJ and **d** DJF. **e**–**h** The same as **a**–**d** except for 1000–500 hPa thickness index. Black dots represent values exceeding the 90% confidence level

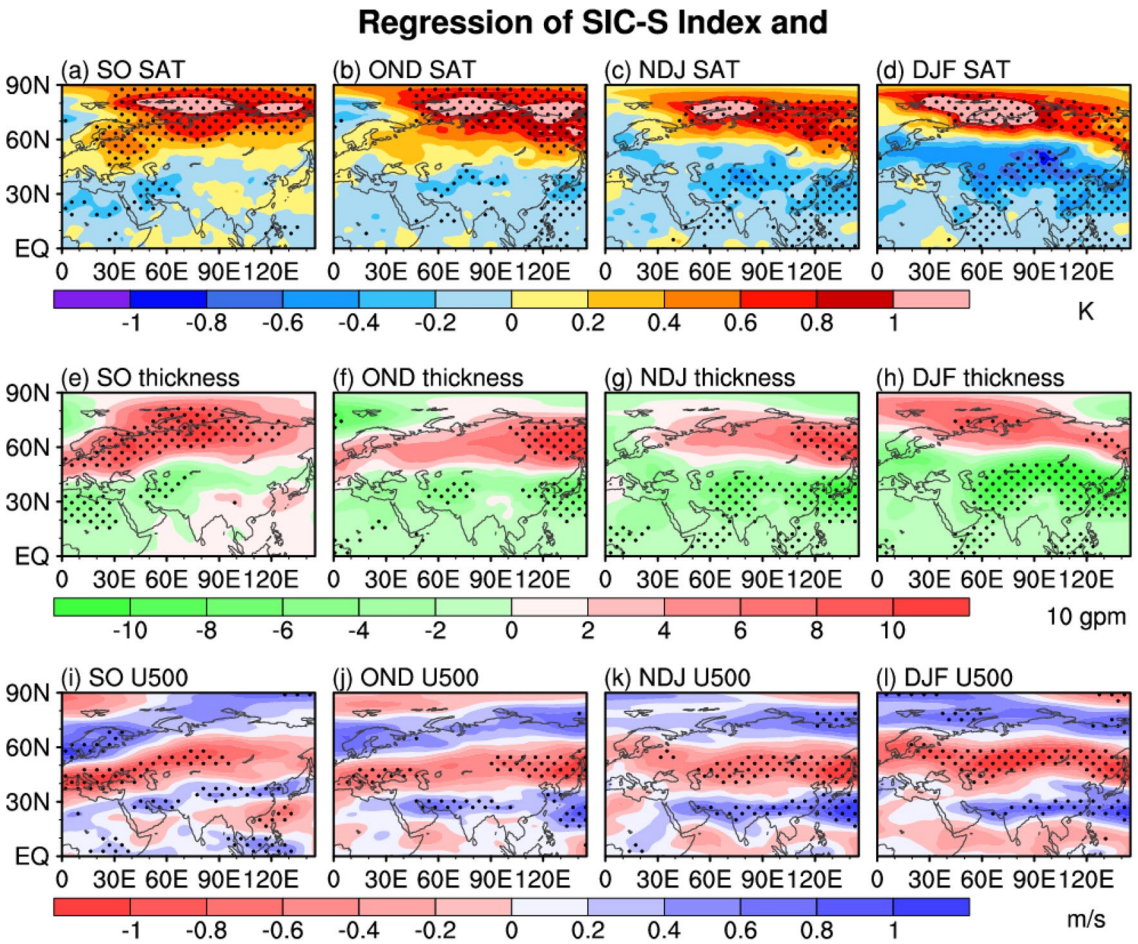

Fig. 9 Same as Fig. 8 except for SIC-S index

propagation of the large-scale Rossby wave moves more slowly when zonal wind decreases. In this case, the abnormal cyclonic (anticyclonic) vorticity over EA (Siberia) is reinforced, indicating an enhanced wave amplitude, causing the development of the troughs and ridges (Palmén and Newton 1969; Holton 2004). Owing to the polar front jet extend from western Europe eastward throughout the entire mid-high latitude Eurasia with their cores exhibiting a different meridional location. The resultant EA trough (Siberian high) for SIC-S shifts (extends) more southeastward than that of SIC-N. As such, the resultant EA trough (Siberian high) for SIC-S shifts (extends) more southeastward than that of SIC-N, leading to an SAT S-mode or N-mode of EAWM.

5 Empirical prediction of the two SAT leading modes of EAWM

It is widely believed that ENSO and Eurasian snow cover are the important predictors for the EAWM (Lee et al. 2013; Luo and Wang 2018), and they exert different connections with the two leading modes of EAWM (Wang et al. 2010). The results above indicate that the autumn Arctic sea ice offers an additional physical-based predictor for the two modes of EAWM beside Eurasian snow cover and ENSO. To examine how well the autumn sea ice in the Arctic contributes to the prediction skill of the two leading modes, the statistical prediction models are established applying a linear regression method based on autumn SIC-N and SSSC for N-mode and SIC-S and ENSO for the S-mode for 1979–2014. We apply the cross-validation approach to check the predictive capability of the statistical models. The leave-nine-out strategy is chosen to guarantee a robust hindcast result. Follow the steps outlined below: the cross-validation method discards 9 years from 1979 to 2014 in proper order, trains the prediction model with the residual years, and exams it on the removal cases. It should be pointed out that leaving out nine is based on the suggestion of Blockeel and Struyf (2002), who believed randomly selecting 70–80% of the data to be the training set for conducting regression and the rest as in a test data would avoid overfitting and wasting data. In this research, 25% of the entire period (36 years) equals

to 9 years. This is the reason for choosing a leave-nine-out strategy. The TCC between the prediction and observation is calculated as the skill score to appraise the performance of the model.

Figure 10a shows the cross-validated estimates of the N-mode of the EAWM. The TCC between the observed N-mode index (black curve) and the 36-year cross-validated estimates of the statistical model based on SIC-N and SSSC indices (red curve) reaches 0.71. If we constructed the prediction model only with the SO SIC-N index and performed the same hindcast (yellow curve), their TCC would be 0.64, which is much higher than that of the SON SSSC (green curve, TCC is 0.30, significant at 90% confidence level). It implies that the SIC-N index does significantly enhance the seasonal prediction capability of the statistical model, and providing a better predictor than the SSSC. For the cross-validated estimates of the S-mode (Fig. 10b), it shows that if we constructed the prediction model with ENSO, the TCC between the observed S-mode index (black curve) and the statistical model (green curve) is only 0.18, not exceeding the 90% confidence level. However, the TCC runs up to 0.61 when the SIC-S is introduced in (yellow curve) and to 0.60 when both ENSO and SIC-S are used (red curve) to establish the prediction model. Why cannot ENSO provide a good predictor to forecast the SAT S-mode of EAWM? It can partly attribute to the ENSO diversity (Capotondi et al. 2015; Zhang et al. 2019b) and the decadal variation of ENSO itself, leading to an unstable relationship between ENSO and EAWM (He and Wang 2013; Jia et al. 2016). Besides, on account of the insignificant correlation between S-mode and NESSC index for 1979–2014 (Fig. 1d), the NESSC index is not applied to construct the prediction model for the S-mode.

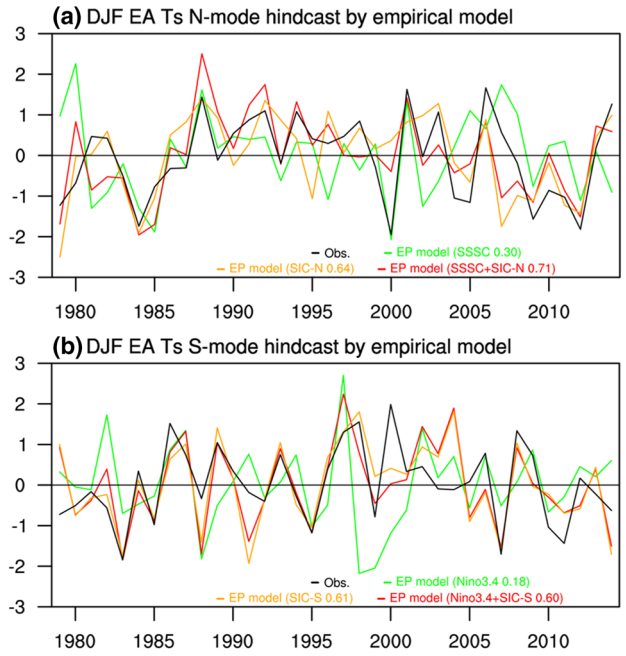

Fig. 10 Comparison of the hindcast winter EA SAT N-mode (**a**) and S-mode (**b**) made by the empirical model

Further examines the prediction skills of the sea ice indexes in the four key regions (not shown). For the N-mode, the prediction skills of BK and northern-CB indices are 0.47 and 0.31, respectively. For the S-mode, the prediction skills of BKL and southern-CB indices are 0.55 and 0.39. Demonstrating the prediction skill of a single sea ice index is lower than the combined indices. Furthermore, in the real-time sea ice concentration and snow cover being monitored day by day, the empirical modes established with Arctic sea ice and Siberian snow cover can be introduced into the practical forecast for the two SAT modes of EAWM.

6 Conclusion and discussion

Many studies have revealed that autumn Arctic sea ice exerts a great impact on the EAWM (Honda et al. 2009; Sun et al. 2016; Wu et al. 2015; Zuo et al. 2016). However, due to the large meridional extent, EAWM is dominated by the SAT northern and the southern modes. Although it has been found that preceding Siberian snow cover anomalies and ENSO, contribute to the inter-annual variations of these two modes (Wang et al. 2010; Chen et al. 2014; Zhang et al. 2019a), whether and how preceding autumn Arctic sea ice affect them are still unclear. We put forward observed evidence in this study that the cold phase of the SAT N-mode can be attributed to the autumn sea ice loss in the BK and North CB Sea (SIC-N), but the cold phase of S-mode is related to the reduced sea ice in the BKL Sea and excessive sea ice in the South CB Sea (SIC-S). We also uncovered the autumn SIC-N and SIC-S anomalies, which can explain approximately 41% and 40% of the variance of the SAT N-mode and S-mode for the period of 1979–2017.

Further analysis implied that the abnormal autumn sea ice in the Eurasian Arctic and CB Sea exert different impact on the winter atmospheric anomalies. In general, the sea ice reduced in BK or BKL Sea in autumn usually induces an enhanced EA trough and a reinforced Siberian high. In this situation, the EA continent is dominated by a colder than normal SAT. However, the autumn sea ice anomalies in the CB Sea play different roles. The sea ice loss in the N-CB Sea usually induces a negative Z500 anomaly located over the Lake Baikal and positive Z500 and SLP anomalies centered over the Ural region, which opposites with that of positive S-CB sea ice anomalies. When the sea ice decrease over the BK and N-CB Sea in autumn (SIC-N anomalies), a significantly reinforced Siberian high and a northwestward shifted EA trough appear in the following winter, which results in a colder than normal conditions mainly over the north of

40° N. However, when the autumn sea ice reduced in the BKL Sea but increased in the S-CB (SIC-S anomalies), the resultant Siberian high became weaker but extended more southward than that of SIC-N, meanwhile, the deepened EA trough centered over southern Japan. These situations favor the mid-high latitude cold air mass invading into the South China Sea, leading to a colder than normal winter over the south of 40° N. Therefore, the autumn sea ice conditions over the CB Sea modulate the influences of abnormal Eurasian Arctic sea ice on the SAT leading modes.

We further found that the autumn SIC-N anomalies tend to significantly enhance the simultaneous SAT and the 1000–500-hPa thickness over the eastern Arctic. Such anomalies sustain from autumn to the following winter, decreasing the meridional thickness gradient between North Continent and the eastern Arctic, resulting in a weaker PFJ which prevailing to the north of 55° N. On the other hand, the autumn SIC-S anomalies favor to increase the anomalous SAT and 1000–500-hPa thickness over the Eurasian Arctic and northern Siberia regions from fall to winter, reducing the meridional thickness gradient between mid- to low-latitude Eurasia and the southern Arctic and inducing a weaker than normal PFJ which blowing along the 50° N in winter. The meridional shift of PFJ moves the centers of the Siberian High and the EA through, inducing different SAT modes of EAWM.

Since the low TCCs between SIC-N index and South Siberian snow cover (0.05), between the SIC-S index and ENSO (0.1), they may act as the new predictability sources for the SAT leading modes of EAWM. According to this evidence, we further inspected the prospective predictability of the two leading modes from the abnormal Arctic sea ice in fall by establishing an empirical prediction model in which the anomalous autumn Arctic sea ice, ENSO and southern Siberian snow cover are used as the predictors. The results from the leave-nine-out cross-validation approach for the period of 1979–2014 suggest that the model shows a relatively low hindcast skill for SAT N-mode of EAWM by considering the SSSC as a predictor, but displays considerable skill by introducing the SIC-N or both the SIC-N and SSSC as the predictors. For the S-mode, the SIC-S anomalies provide an appreciable hindcast skill, which much higher than that of ENSO. Therefore, comparing with ENSO and Siberian snow cover, the SIC-N and SIC-S-based statistical model offers a better forecast system and may promote the seasonal prediction of the two SAT leading modes of EAWM.

The statistical prediction models are based on the seasonal mean time-scale in this study. However, many extreme events with great impact have a strong sub-seasonal feature. Do the leading modes of extreme SAT on the sub-seasonal time scale over EA exhibit the spatial patterns that resemble the northern and southern mode? If yes, whether the SIC-N and SIC-S anomalies can be introduced into predict these sub-seasonal modes? If not, what are their new predictability sources? These questions need further discussions. Besides, the influencing processes of SIC-N and SIC-S anomalies, especially the potential effects of the sea ice over Chukchi–Beaufort onto the N- and S-modes require detailed numerical and theoretical studies.

Acknowledgements We thank the two anonymous reviewers for their comments and suggestions. This research was jointly supported by the National Natural Science Foundation of China (Grant Nos. 41790475, 41905056 and 91937302) and the Ministry of Science and Technology of China (Grant No. 2016YFA0601801).

References

Blockeel H, Struyf J (2002) Efficient algorithms for decision tree cross-validation. J Mach Learn Res 3:621–650

Budikova D (2009) Role of Arctic sea ice in global atmospheric circulation: a review. Glob Planet Change 68:149–163

Capotondi A et al (2015) Understanding ENSO diversity. Bull Am Meteorol Soc 96:921–938

Chen W, Graf HF, Huang RH (2000) The interannual variability of East Asian winter monsoon and its relation to the summer monsoon. Adv Atmos Sci 17:46–60

Chen Z, Wu R, Chen W (2014) Impacts of autumn Arctic sea ice concentration changes on the East Asian winter monsoon variability. J Clim 27:5433–5450

Chevallier M, Salas-Melia D (2012) The role of sea ice thickness distribution in the Arctic sea ice potential predictability: a diagnostic approach with a coupled GCM. J Clim 25:3025–3038

Clark MP, Serreze MC (2000) Effects of variations in East Asian snow cover on modulating atmospheric circulation over the North Pacific Ocean. J Clim 13:3700–3710

Cohen J, Screen JA, Furtado JC et al (2014) Recent Arctic amplification and extreme mid-latitude weather. Nat Geos 7:627

Comiso JC (2012) Large decadal decline of the Arctic multiyear ice cover. J Clim 25:1176–1193

Dee DP et al (2011) The ERA-Interim reanalysis: configuration and performance of the data assimilation system. Q J R Meteorol Soc 137:553–597

Ding YH (1994) Monsoon over China. Kluwer Academic, Dordrecht, p 420

Estilow TW, Young AH, Robinson DA (2015) A long-term Northern Hemisphere snow cover extent data record for climate studies and monitoring. Earth Syst Sci Data 7:137–142

Francis JA, Vavrus SJ (2012) Evidence linking Arctic amplification to extreme weather in mid-latitudes. Geophys Res Lett 39:L06801

Francis JA, Chan W, Leathers DJ, Miller JR, Veron DE (2009) Winter Northern hemisphere weather patterns remember summer Arctic sea-ice extent. Geophys Res Lett 36:L07503

Gong G, Entekhabi D, Cohen J (2003) Modeled Northern Hemisphere winter climate response to realistic Siberian snow anomalies. J Clim 16:3917–3931

He SP, Wang HJ (2013) Oscillating relationship between the East Asian Winter monsoon and ENSO. J Clim 26:9819–9838

Holton JR (2004) An introduction to dynamic meteorology, 4th edn. Elsevier Academic Press, Oxford

Honda M, Inoue J, Yamane S (2009) Influence of low Arctic sea-ice minima on anomalously cold Eurasian winters. Geophys Res Lett 36:L08707

Hopsch S, Cohen J, Dethloff K (2012) Analysis of a link between fall Arctic sea ice concentration and atmospheric patterns in the following winter. Tellus A 64:18624

Inoue J, Hori ME, Takaya K (2012) The role of Barents Sea ice in the wintertime cyclone track and emergence of a warm-Arctic cold–Siberian anomaly. J Clim 25:2561–2568

Jhun J-G, Lee E-J (2004) A new East Asian Winter Monsoon Index and associated characteristics of the Winter Monsoon. J Clim 17:711–726

Jia X, Lin H, Ge J (2016) The interdecadal change of ENSO impact on wintertime East Asian climate. J Geophys Res 120:11918–11935

Koenigk T, Caian M, Nikulin G, Schimanke S (2016) Regional Arctic sea ice variations as predictor for winter climate conditions. Clim Dyn 46:317–337

Kug JS, Jeong JH, Jang YS, Kim BM, Folland CK, Min SK, Son SW (2015) Two distinct influences of Arctic warming on cold winters over North America and East Asia. Nat Geol 8:759

Lau KM, Li MT (1984) The monsoon of East Asia and its global associations—a survey. Bull Am Meteorol Soc 65:114–125

Lee JY, Lee SS, Wang B, Ha KJ, Jhun JG (2013) Seasonal prediction and predictability of the Asian winter temperature variability. Clim Dyn 41:573–587

Li F, Wang H (2014) Autumn Eurasian snow depth, autumn Arctic sea ice cover and East Asian winter monsoon. Int J Climatol 34:3616–3625

Liu G, Ji LR, Sun SQ, Xin YF (2012) Low- and midhigh latitude components of the East Asian winter monsoon and their reflecting variations in winter climate over eastern China. Atmos Ocean Sci Lett 5:195–200

Lu MM, Chang C-P (2009) Unusual late-season cold surges during the 2005 Asian winter monsoon: roles of Atlantic blocking and the central Asian anticyclone. J Clim 22:5205–5217

Luo X, Wang B (2018) How autumn Eurasian snow anomalies affect East Asian winter monsoon: a numerical study. Clim Dyn 52:69–82

Mori M, Watanabe M, Shiogama H, Inoue J, Kimoto M (2014) Robust Arctic sea-ice influence on the frequent Eurasian cold winters in past decades. Nat Geosci 7:869–873

North GR, Bell TL, Cahalan RF, Moeng FJ (1982) Sampling errors in the estimation of empirical orthogonal functions. Mon Weather Rev 110:699–706

Overland JE, Wang M (2010) Large-scale atmospheric circulation changes are associated with the recent loss of Arctic sea ice. Tellus A 62:1–9

Palmén E, Newton CW (1969) Atmospheric circulation systems, international geophysics series, vol 13. Academic, New York

Petoukhov V, Semenov VA (2010) A link between reduced Barents–Kara sea ice and cold winter extremes over northern continents. J Geophys Res 115:D21111

Rayner NA, Parkler DE, Horton EB, Folland CK, Alexander LV, Rowell DP, Kent EC, Kaplan A (2003) Global analyses of sea surface temperature, sea ice, and night marine air temperatures since the late nineteenth century. J Geophys Res 108(D14):4407

Robinson DA, Frei A (2000) Seasonal variability of northern hemisphere snow extent using visible satellite data. Prof Geogr 51:307–331

Robinson DA, Dewey KF, Heim R Jr (1993) Global snow cover monitoring: an update. Bull Am Meteorol Soc 74:1689–1696

Screen JA (2014) Arctic amplification decreases temperature variance in northern mid-to high-latitudes. Nat Clim Change 4:577

Screen JA, Simmonds I (2013) Exploring links between Arctic amplification and mid-latitude weather. Geophys Res Lett 40:959–964

Solomon S, Qin D, Manning M, Marquis M, Averyt K, Tignor MMB, Miller HL, Chen Z (2007) Climate change 2007—the physical science basis: working group I contribution to the fourth assessment report of the IPCC, vol 4. Cambridge University Press, Cambridge

Stroeve JC, Maslanik J, Serreze MC, Rigor R, Meier W, Fowler C (2011) Sea ice response to an extreme negative phase of the Arctic Oscillation during winter 2009/2010. Geophys Res Lett 38:L02502

Sun C, Yang S, Li W, Zhang R, Wu R (2016) Interannual variations of the dominant modes of East Asian winter monsoon and possible links to Arctic sea ice. Clim Dyn 47:481–496

Tang Q, Zhang X, Yang X, Francis JA (2013) Cold winter extremes in northern continents linked to Arctic sea ice loss. Environ Res Lett 8:014036

Tao SY, China Meteorological administration (1957) A study of activities of cold airs in East Asian winter. Handbook of short-term forecast. Meteorology Press, Beijing, pp 60–92 **(in Chinese)**

Vihma T (2014) Effects of Arctic sea ice decline on weather and climate: a review. Surv Geophys 35:1175–1214

Wang L, Chen W (2010) How well do existing indices measure the strength of the East Asian winter monsoon? Adv Atmos Sci 27:855–870

Wang L, Chen W (2014) An intensity index for the East Asian winter monsoon. J Clim 27:2361–2374

Wang B, Wu R, Fu X (2000) Pacific-East Asia teleconnection: how does ENSO affect East Asian climate? J Clim 13:1517–1536

Wang L, Chen W, Huang RH (2008) Interdecadal modulation of PDO on the impact of ENSO on the East Asian winter monsoon. Geophys Res Lett 35:L20702

Wang B, Lee JY, Kang IS, Shukla J, Park CK, Kumar A et al (2009) Advance and prospectus of seasonal prediction: assessment of the APCC/CliPAS 14-model ensemble retrospective seasonal prediction (1980–2004). Clim Dyn 33:93–117

Wang B, Wu Z, Chang CP, Liu J, Li J, Zhou T (2010) Another look at interannual-to-interdecadal variations of the East Asian winter monsoon: the northern and southern temperature modes. J Clim 23:1495–1512

Wu B, Huang RH, Gao DY (1999) Impact of variations of winter sea-ice extents in the Kara/Barents Seas on winter monsoon over East Asia. Acta Meteorol Sin 13:141–153 **(in Chinese)**

Wu Z, Li J, Wang B, Liu X (2009) Can the Southern Hemisphere annular mode affect China winter monsoon? J Geophys Res 114:D11

Wu Z, Li J, Jiang Z, He J (2011) Predictable climate dynamics of abnormal East Asian winter monsoon: once-in-a-century snowstorms in 2007/2008 winter. Clim Dyn 37:1661–1669

Wu Z, Li X, Li Y (2016) Potential influence of Arctic sea ice to the inter-annual variations of East Asian spring precipitation. J Clim 29:2797–2813

Wu B, Su J, D'Arrigo R (2015) Patterns of Asian winter climate variability and links to Arctic sea ice. J Clim 28:6841–6858

Yu L, Wu Z, Zhang R, Yang X (2018) Partial least regression approach to forecast the East Asian winter monsoon using Eurasian snow cover and sea surface temperature. Clim Dyn 51:4573–4584

Zhang X, Walsh JE (2006) Toward a seasonally ice-covered Arctic Ocean: scenarios from the IPCC AR4 model simulations. J Clim 19:1730–1747

Zhang R, Sumi A, Kimoto M (1996) Impact of El Niño on the East Asian monsoon: a diagnostic study of the '86/87 and '91/92 events. J Meteorol Soc Jpn 74:49–62

Zhang X, Sorteberg A, Zhang J, Gerdes R, Comiso JC (2008) Recent radical shifts of atmospheric circulations and rapid changes in Arctic climate system. Geophys Res Lett 35:L22701

Zhang P, Wu ZW, Chen H (2017) Interdecadal variability of the ENSO–North Pacific atmospheric circulation in winter. Atmos Ocean 55(2):110–120

Zhang J, Stegall ST, Zhang X (2018) Wind–sea surface temperature–sea ice relationship in the Chukchi–Beaufort Seas during autumn. Environ Res Lett 13:034008

Zhang P, Wu ZW, Li JP (2019a) Reexamining the relationship of La Niña and the East Asian Winter Monsoon. Clim Dyn 53:779–791

Zhang P, Wang B, Wu ZW (2019b) Weak El Niño and Winter climate in the mid-to high latitudes of Eurasia. J Clim 32:405–421
Zuo J, Ren HL, Wu B, Li W (2016) Predictability of winter temperature in China from previous autumn Arctic sea ice. Clim Dyn 47:2331–2343